ResearchGate

See discussions, stats, and author profiles for this publication at: https://www.researchgate.net/publication/257422627

Chain Length Effects on the Dynamics of Poly(ethylene oxide) Confined in Graphite Oxide: A Broadband Dielectric Spectroscopy Study

ARTICLE *in* MACROMOLECULES · OCTOBER 2013

Impact Factor: 5.8 · DOI: 10.1021/ma401373p

CITATIONS
4

READS
61

4 AUTHORS, INCLUDING:

Fabienne Barroso-Bujans
Center of Materials Physics
45 PUBLICATIONS **733** CITATIONS
SEE PROFILE

Silvina Cerveny
Universidad del País Vasco / Euskal Herriko U…
55 PUBLICATIONS **1,043** CITATIONS
SEE PROFILE

Juan Colmenero
Universidad del País Vasco / Euskal Herriko U…
401 PUBLICATIONS **8,521** CITATIONS
SEE PROFILE

Available from: Silvina Cerveny
Retrieved on: 27 January 2016

Macromolecules

Article

pubs.acs.org/Macromolecules

Chain Length Effects on the Dynamics of Poly(ethylene oxide) Confined in Graphite Oxide: A Broadband Dielectric Spectroscopy Study

Fabienne Barroso-Bujans,*[,†,‡] Silvina Cerveny,[†] Ángel Alegría,[†,§] and Juan Colmenero[†,‡,§]

[†]Centro de Física de Materiales-Material Physics Center (CSIC-UPV/EHU), Paseo Manuel Lardizábal 5, 20018 San Sebastian, Spain

[‡]Donostia International Physics Center (DIPC), Paseo Manuel Lardizábal 4, 20018 San Sebastian, Spain

[§]Departamento de Física de Materiales, Universidad del País Vasco (UPV/EHU), Apartado 1072, 20080 San Sebastian, Spain

Supporting Information

ABSTRACT: The dynamics of poly(ethylene oxide) (PEO) intercalated in the subnanometer-spaced graphite oxide (GO) layers is investigated by using broadband dielectric spectroscopy (BDS). To this end, we compare BDS data obtained for PEO chains of increasing lengths, from three monomeric units to several thousand repetitive ethylene oxide units (n = 3−2135). Two relaxations were clearly identified for the confined PEO. The slowest one is proposed to originate from interfacial polarization. It is dependent on the chain length and exhibits a change in activation energy at 247 K, a temperature at which the GO exhibits an interlayer expansion when subjected to an increase in temperature. The fastest relaxation is nearly independent of the chain length, in contrast to the behavior that we found for the β-relaxation of bulk PEO. These results strengthen a previous hypothesis suggesting the emergence of a new set of chain length scales primarily dictated by the presence of anchoring points on the GO substrate upon intercalation. Additionally, the fastest relaxation exhibits a crossover at 175 K, which indicates the coexistence of two distinct processes, one occurring with the same activation energy as in the bulk polymer, and the other with lower activation energy. The latter is probably associated with the planar zigzag conformation in the confined PEO as previously determined by high-resolution inelastic neutron scattering.

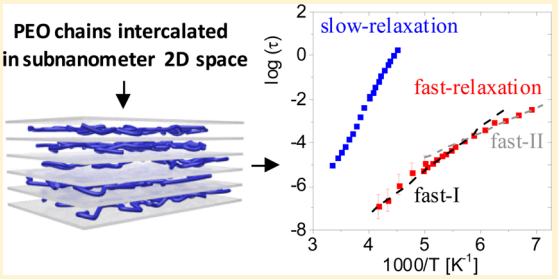

1. INTRODUCTION

The glass transition (the freezing of a supercooled liquid into an amorphous solid) is a phenomenon in which the dynamics of a liquid slows down as the temperature decreases. However, this important aspect of condensed matter physics is not yet fully understood.[1−3] The most prominent experimental feature of the glass transition is the rapidly increasing viscosity, or the related relaxation time, of the main (or α) relaxation as the temperature decreases toward the glass transition temperature, T_g. By confining small molecules or macromolecules in very small spaces, one hopes to find additional information about the underlying physics, such as the possible existence of a length scale associated with molecular motions responsible for the glass transition. The growth of the correlation length as the temperature decreases may be responsible for the slowing-down of the dynamics.[4,5] For these reasons, in the last 2 decades, the dynamics of glass forming systems or polymers close to interfaces, in thin films, or confined in nanopores has been intensively studied with the aim of increasing the understanding of the glass transition.[6−9]

However, the influence of spatial confinement on the dynamics of polymers is still inadequately understood. Different types of confinement have been employed such as thin films,[10−17] porous materials (zeolites,[18,19] MCM-41,[20] vermiculite clays,[21,22] and montomorillonites[23]), aluminum-oxide templates,[24,25] polymer nanoparticles,[26] blends,[27,28] block copolymers,[29] and polymer assemblies,[30] with the aim of exploring the influence of dimensionality on the dynamics of the confined systems. In addition, another important factor in these studies is the interaction with the host system. Depending on the nature of the interfacial interactions (e.g., hydrophilic or hydrophobic) the relaxation dynamics will either slow down or speed up.[8,9]

In this context, graphite oxide (GO) offers unique opportunities as a host material for studying the dynamical behavior of molecules and macromolecules in two-dimensional (2D) confinement at the subnanometer scale. The primary advantage of using GO as a host lies in the ability to control and tune its degree of oxidation and exfoliation and, therefore, the strength of the interaction between host and intercalated species.[31,32] GO is highly hydrophilic as expected from its high oxygen content in the interlamellar regions. This characteristic guarantees the intercalation of hydrophilic species in the

Received: July 2, 2013
Revised: September 11, 2013
Published: September 27, 2013

ACS Publications © 2013 American Chemical Society

interlayer such as water,[33−36] electrolyte solutions,[37] alcohols,[38] and polyethers,[39,40] among others.

In a recent study, we have investigated the dynamics and structure of poly(ethylene oxide) (PEO) of high molecular weight, Mn =10^5 g/mol, confined in an interlayer space of 9.1 Å in GO.[39] Calorimetric experiments showed that in this confinement space, the crystallization and glass transition of PEO are suppressed as a result of strong geometric restrictions (the polymer phase was confined to a monolayer of about 3.4 Å). In addition, the dynamics of PEO confined in GO, as studied by broadband dielectric spectroscopy (BDS),[39] showed a suppression of the α-relaxation. These results were rationalized in terms of the cooperativity suppression among polymer chains and restricted chain motions induced by strong hydrogen-bond interactions between PEO ethers and GO hydroxyls. By means of high resolution inelastic neutron spectroscopy (INS),[40] we observed significant changes in both the polymer conformation and the collective vibrational modes as a consequence of a predominant planar zigzag (*trans*−*trans*−*trans*) chain conformation in the confined polymer, which departed significantly from the characteristic 7/2 helical structure of the bulk crystal. Surprisingly, these effects were largely insensitive to polymer chain length suggesting the emergence of a new set of chain length scales primarily dictated by the presence of anchoring points on the GO substrate upon intercalation.[40]

By means of BDS, we explore in the present work how the dynamics of PEO of varying chain lengths is affected by the extreme 2D confinement in the interlayer space of GO. Two relaxation processes are observed for confined PEO. The slowest one depends on chain length and seems to be associated with interfacial polarization. This assignment is further corroborated by the fact that this relaxation exhibits a change in the activation energy at the same temperature at which the GO undergoes an interlayer expansion when subjected to an increase in temperature. On the contrary, the fastest relaxation is nearly independent of the chain length, in contrast to the behavior that we observed for the β-relaxation of the bulk polymer. Additionally, the fast-relaxation exhibits an unexpected crossover in temperature dependence at about 175 K. These results are interpreted as originating from a simultaneous contribution of two distinct local molecular motions: one with a similar activation energy as in the bulk polymer and the other with a lower activation energy.

2. EXPERIMENTAL METHODS

2.1. Synthesis of Graphite Oxide. Graphite oxide was produced using natural graphite from Alfa Aesar (universal grade, 200-mesh, 99.9995% metal basis, reference number 40799). The starting graphite material was oxidized using a modified Brodie method.[40,41] A reaction flask containing 200 mL of fuming nitric acid (Fluka) was cooled to 0 °C for 20 min using a cryostat bath, followed by the immersion of 10 g of graphite. Next, 80 g of potassium chlorate (Fluka) was slowly added over a period of 1 h in order to avoid sudden increases in temperature. The reaction mixture was stirred for 21 h at 0 °C. The mixture was then diluted in distilled water and filtered until the supernatant had a nitrate content below 1 mg/L. The resulting GO slurry was dried at 80 °C for 24 h in a vacuum oven (P < 0.1 mbar) and stored in this oven at room temperature until further use. Elemental analysis of the so-obtained GO showed an atomic composition of $C_8H_{1.3}O_{2.6}$.

2.2. Preparation of Graphite−Oxide Intercalates. Triethylene glycol (3PEO) and pentaethylene glycol (5PEO) were purchased from Fluka, and *n*PEOs (with n = 13, and 104) were supplied by Aldrich. These materials have the chemical formula H−(O−CH_2−CH_2)$_n$−OH with n varying as shown in Table 1. Number-average molecular weights, Mn, are also given.

Table 1. Bulk Samples Used in This Study, Where n is the Degree of Polymerization[a]

sample	n	M_n [g/mol]	T_g (DSC) [K]
3PEO	3	150	181.5
5PEO	5	238	191.1
13PEO	13	590	209.5
104PEO	104	4600	219.5

[a]T_g (DSC) represents the onset of the heat flow during a heating run measured by DSC at 10 K/min.

*n*PEO-GO samples with n = 13 and 104 were prepared from aqueous solution by stirring a total of 0.5 g of PEO previously dissolved in 20 mL of water with 0.5 g of GO for 15 days. Any PEO excess was removed by filtration and thorough aqueous washings. The resulting *n*PEO-GO specimen was then dried at 80 °C for 24 h in a vacuum oven (P < 0.1 mbar) connected to a dry scroll rotatory pump. *n*PEO-GO, GO, and *n*PEO were kept dry in the vacuum oven at room temperature prior to their physicochemical characterization. The intercalation of 3PEO and 5PEO (all of them are liquids at ambient temperature) was performed by direct mixing with GO in the absence of solvent. To remove any remaining liquid, the adduct was carefully rinsed with water and dried at 80 °C under vacuum. As a precautionary measure, all samples were analyzed by termogravimetric analysis (TGA) and differential scanning calorimetry (DSC) to identify the presence of excess liquid. The drying procedure explained earlier was performed repeatedly to achieve the complete removal of the nonintercalated fraction. A final composition of ca. 22 wt % (±2 wt %) *n*PEO in the *n*PEO-GO samples was ascertained by means of TGA and further corroborated by the INS measurements.[40] The interlayer space of PEO intercalated in GO is around 9 Å. Additional compositional information can be found in reference.[40]

2.3. Thermal Characterization. A DSC Q2000 TA Instrument was used in standard mode. A cooling−heating cycle between T_g − 50 K and T_g + 50 K with rates of 10 K/min was performed. Hermetic aluminum pans were used for all materials. A helium flow rate of 25 mL/min was used throughout. The annealing time between cooling and heating runs was 2 min. From the heat flow/temperature curves, T_g values were calculated at the onset point.

2.4. Broadband Dielectric Spectroscopy. A broadband and high-resolution dielectric spectrometer, Novocontrol Alpha, was used to measure the complex dielectric function, $\varepsilon^*(\omega) = \varepsilon'(\omega) - i\,\varepsilon''(\omega)$, $\omega = 2\pi f$, in the frequency (f) range from $f = 10^{-2}$ Hz to $f = 10^6$ Hz. Liquid (n = 3, 5, and 13) and solid (n = 104 and 2135) bulk *n*PEO samples were placed between parallel gold-plated electrodes which were 30 mm in diameter and 0.1 mm thick. In order to avoid crystallization during cooling, samples were quenched by immersion into liquid nitrogen. In the case of solid *n*PEO samples, they were previously molten at 353 K before quenching. Powder *n*PEO-GO samples were placed between two parallel gold-plated electrodes of 30 mm diameter and 0.5 mm thickness. In contrast to bulk samples, confined samples do not present any crystallization on cooling or heating and therefore quenching is not necessary. All samples were measured isothermally during heating every fifth degree over 140−180 K and every third degree over 183−250 K. Sample temperature was controlled with stability better than ±0.2 K.

For the analysis of the dielectric measurements, we have used the Havriliak−Negami function (HN)[42] to fit the imaginary part ε'' of the dielectric function:

$$\varepsilon^*(\omega) = \varepsilon_\infty + \frac{\Delta\varepsilon}{[1 + (i\omega\tau)^\alpha]^\gamma} \quad (1)$$

where $\Delta\varepsilon = \varepsilon_s - \varepsilon_\infty$, ε_∞, and ε_s are the unrelaxed and relaxed values of the dielectric constant, τ is the relaxation time and ω is the angular frequency. In eq 1 α and γ are shape parameters ($0 < \alpha$, $\alpha\gamma \leq 1$).

dx.doi.org/10.1021/ma401373p | *Macromolecules* 2013, 46, 7932−7939

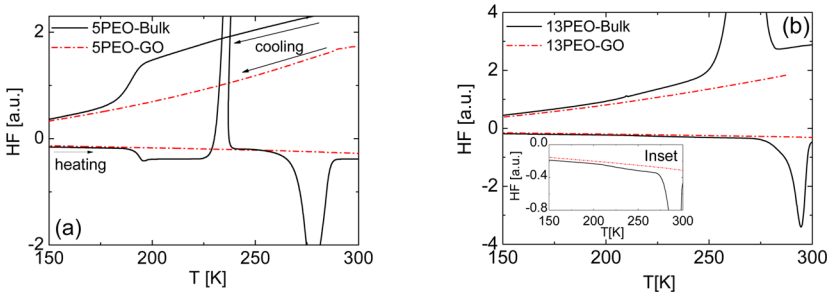

Figure 1. (a) Heat flow measured by DSC of 5PEO-bulk (filled line) and 5PEO confined in GO (5PEO-GO, dotted line) during cooling and heating runs at a rate of 10 K/min. Crystallization on heating is avoided in the confined 5PEO. (b) Heat flow measured by DSC of 13PEO-bulk (filled line) and 13PEO confined in GO (dotted line) during cooling and heating runs at a rate of 10 K/min. Crystallization on cooling is present on bulk 13PEO and a broad glass transition on heating is observed (see the inset figure). Crystallization and glass transition are not observed in confined 13PEO.

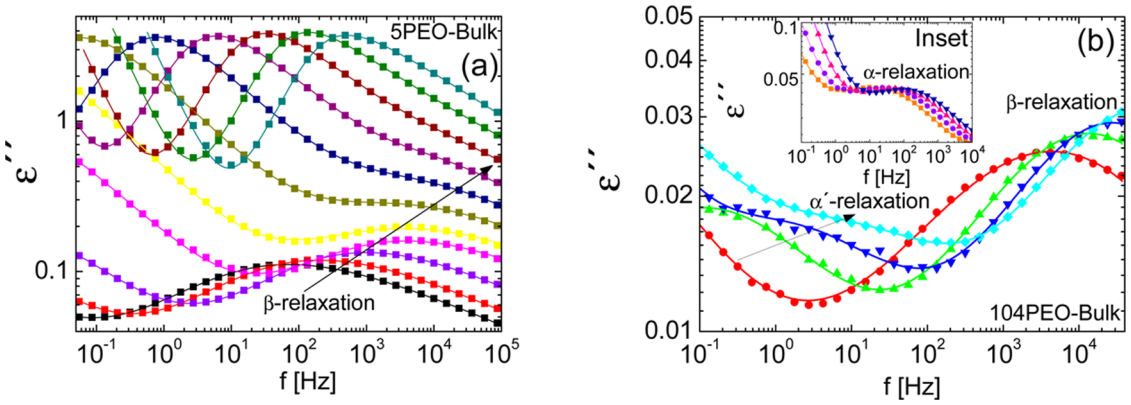

Figure 2. (a) Dielectric loss spectra of 5PEO-bulk measured at different temperatures (160, 165, 175, 186, 189, 201, 204, and 207 K). (b) Dielectric loss spectra of 13PEO-bulk measured at different temperatures (170, 183, 192, 201 K). Inset: Same as in part b at 243, 246, 249, and 252 K. In both parts a and b, the solid line through the data points represents the fits to the experimental data.

Setting $\gamma = 1$, a symmetrical function is obtained (Cole−Cole (CC) function[43]) which is widely used to describe secondary relaxations in glassy materials. In addition, at low frequencies/high temperatures conductivity effects dominate and, to account for that, a power law term was added.

2.5. X-ray Diffraction. X-ray diffraction (XRD) patterns were measured using a Bruker D8 Advance powder diffractometer equipped with a Cu Kα radiation source (λ = 1.54 Å), a LynxEye detector and an Anton-Paar TTK450 temperature stage. The radiation source was operated at a generator voltage of 40 kV and a current of 40 mA. XRD data were collected in the temperature range of 133−353 K over the angular range 2θ = 5−60° with a step size of 0.026° in Bragg−Brentano parafocusing geometry. Interlayer spacings (d) of pristine GO and *n*PEO-GO samples were obtained from the sharp and intense (001) Bragg reflections[40] for all the temperatures.

3. RESULTS

3.1. Thermal Behavior. Representative DSC scans showing the heat flow of both confined and bulk PEO samples during cooling and heating runs for 5PEO and 13PEO are given in Figure 1, parts a and b. First of all, we will focus on results obtained for bulk samples. At a cooling rate of 10 K/min, it is possible to avoid crystallization in 5PEO-bulk obtaining a glass phase at low temperatures. The heating scan in Figure 1a shows a glass transition temperature (T_g) followed by a cold crystallization at about 230 K. After that, a broad melting transition is observed in the temperature range between 255 and 290 K. 3PEO-bulk presented the same behavior as 5PEO-bulk. On the contrary, samples with higher chain length (13PEO and 104PEO) crystallize during cooling (Figure 1b) obtaining a partially crystallized polymer at low temperatures. However, a small step in the heat flow related to the glass transition of the amorphous fraction of 13PEO is still possible to observe (Inset of Figure 1b). T_g′s corresponding to the amorphous bulk samples (3PEO and 5PEO), as well as the partially crystallized PEO of higher chain lengths, were determined in the onset of the heat flow step. The resulting *Tg* values are shown in Table 1. Although it is generally observed that crystallization has the effect of broadening, weakening and shifting the T_g to higher temperatures, T_g values corresponding to bulk PEO′s are still dependent on the molecular weight in the range investigated.

In contrast to bulk polymers (see dotted line in Figure 1), confined *n*PEO showed no calorimetric features at all. This result indicates that crystallization can be inhibited upon confinement, in agreement with previous studies on PEO intercalated in montmorillonite[23,44] and fluoromica-based clays,[45] among others. On the other hand, the absence of any sign of the calorimetric glass transition could be related to the presence of an extremely broad distribution of segmental relaxation times, and thereby, of glass transition temperatures (see Discussion), as observed in a recent study on PEO confined in nanoporous alumina.[25]

3.2. Dynamical Behavior. In the following sections, we present the dielectric response of bulk amorphous polymers (3PEO and 5PEO) and partially crystallized bulk polymers (13PEO and 104PEO), followed by the dielectric response of confined PEO samples.

3.2.1. Amorphous and Semicrystalline Bulk Samples. Isotherms representing the dielectric loss, $\varepsilon''(f)$, of bulk

dx.doi.org/10.1021/ma401373p | *Macromolecules* 2013, 46, 7932−7939

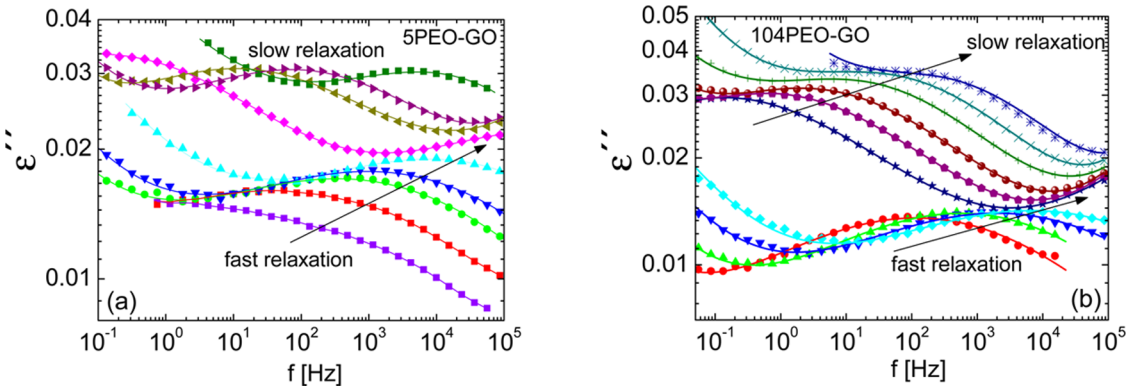

Figure 3. (a) Dielectric loss spectra of 5PEO confined in GO (5PEO-GO) at different temperatures (120, 135, 150, 160, 186, 213, 237, 246 and 280 K). (b) Dielectric loss spectra of 104PEO confined in GO (104PEO-GO) at different temperatures (160, 175, 186, 195, 231, 240, 249, 260, 270 and 285 K). The solid line through the data points represents the fits to the experimental data.

5PEO are shown in Figure 2a. Below the glass transition temperature, the isotherms present a broad β-relaxation. In the vicinity of T_g, isotherms show the α-relaxation in the low-frequency range followed by a shoulder indicative of the remaining contributions of β-relaxation. In this temperature range (from T_g to T_g + 30 K), the contributions to the dielectric loss corresponding to the α- and β-processes are well separated in frequency. Cold crystallization (at about 210 K in the case of 5PEO and at about 215 K for 3PEO) prevents the measurement of the amorphous response of these oligomers at higher temperatures. The dielectric response of both 3PEO and 5PEO was described by using a HN- and a CC-function to take into account the α- and β-relaxations, respectively (see eq 1).

For polymers (n = 13 and 104), crystallization on cooling cannot be avoided and therefore the dielectric measurements reflect the response of semicrystallized polymers. Isotherms of bulk 104PEO are shown in Figure 2b. The observed dielectric spectra show three relaxation processes. The fastest one is the β-relaxation (also observed in amorphous 3PEO or 5PEO) whereas the slower one is the α-relaxation corresponding to the amorphous fraction of 104PEO (see inset). In the middle of these two relaxation processes, we can observe what is usually called α'-relaxation. This is related to the rather local constrained dynamics of PEO chains between crystalline lamellae and interlamellar amorphous PEO.[28] The appearance of a new relaxation has also been observed in other semicrystalline systems such as poly(trimethylene terephthalate),[46] poly(dimethylsiloxane),[47] *trans*-poly(isoprene),[48] and ethylene glycol dimethacrylate.[49] However, in our samples, the α'-relaxation is faster than the α-relaxation, contrary to what was observed in the above-mentioned polymers. Note that in the case of 13PEO-bulk, conductivity masks the α-relaxation and therefore we only observed α'- and β-relaxations. The dielectric response of semicrystalline polymers was described by using three CC functions to take into account the α-, α'- and β-relaxations.

Finally, in order to analyze the dielectric response of semicrystalline bulk samples, we also measured a semicrystalline 5PEO sample. In this way, we can establish how the behavior of the semicrystalline sample compares with the noncrystallized one. Taking advantage of the occurrence of cold crystallization (see Figure 1a), 5PEO was crystallized by maintaining the temperature at 235 K for 1 h. After that, we measured the dielectric response. Figure S1 in the Supporting Information document compares the relaxation times corresponding to the amorphous and semicrystalline sample. We confirmed the presence of a new relaxation corresponding to the so-called α'-relaxation previously shown. The relaxation times corresponding to the β-relaxation are almost unmodified after crystallization (slightly lower in the crystalline sample) whereas the relaxation times corresponding to the α-relaxation become about half a decade faster. We will take into account this information when comparing the dielectric responses of bulk and confined samples.

3.2.2. Confined PEO Samples. We now focus on the dielectric response of confined PEO samples. Parts a and b of Figure 3 show the frequency dependence of the dielectric permittivity $\varepsilon''(\omega)$ of 5PEO confined in GO (5PEO-GO) and 104PEO confined in GO (104PEO-GO) at some temperatures. Two clear relaxations are apparent in both figures. At temperatures below 190 K a single relaxation peak is observed. By increasing the temperature, a second peak emerges on the low-frequency side of the ε'' peak. It must be noted that no calorimetric glass transition was observed by DSC in the confined oligomers (n = 3 and 5), so it is difficult to associate this relaxation with the α-relaxation of bulk samples. As the connection between α- and β-relaxations in bulk with these two relaxations observed in the confined materials is not evident, we will call them "slow" and "fast" relaxations.

According to these results the dielectric response of the confined materials was described by using two CC functions to account for the fast- and slow-relaxations. At higher temperatures a conductivity term was also added.

3.2.3. Relaxation Times of Bulk and Confined Samples. In order to compare different materials in bulk and confined states, we use the peak relaxation time as the most characteristic parameter of the relaxation process.

Figure 4 shows the relaxation time (τ) of the α-, α'- and β-relaxation corresponding to bulk (amorphous or semicrystalline) samples, as obtained from the fitting described in the above section. A direct inspection of this figure shows that the α-process becomes faster for shorter chains. The temperature dependence of τ_α can be well described by the Vogel–Fulcher–Tammann (VFT) equation[50−52]

$$\tau(T) = \tau_o \exp\left(\frac{DT_o}{T - T_o}\right) \quad (2)$$

where τ_o is the high-temperature limit of the relaxation time and T_o the temperature where τ would diverge. Extrapolation of this formula to a relaxation time of τ = 100s usually gives a

dx.doi.org/10.1021/ma401373p | *Macromolecules* 2013, 46, 7932−7939

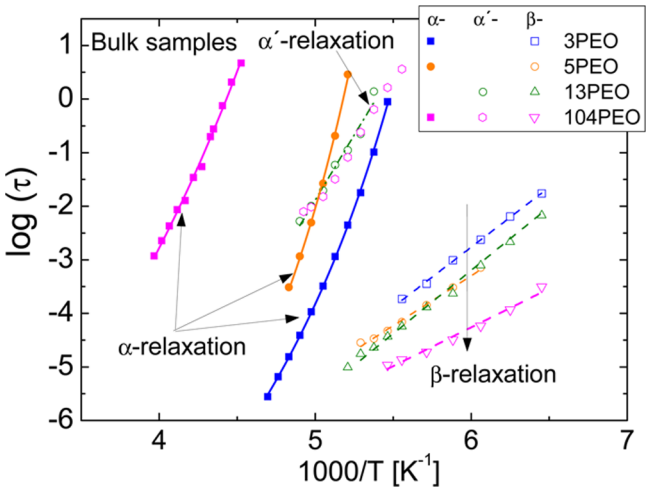

Figure 4. Plot of the characteristic relaxation times of bulk *n*PEO. The solid lines through the data points are fits to the VFT equation while the dotted lines display fits to the Arrhenius equation. In the case of 13PEO and 104PEO, the temperature dependence of α'-relaxation is also displayed (see the text).

dielectric estimate of the glass transition temperature, $T_{g,100s}$. This value and the VFT parameters describing the temperature dependence of the α-relaxation time for bulk samples are given in Table 2.

Table 2. Results from Fits to the VFT Equation for the α-Relaxation of Bulk Samples[a]

n	D	T_o [K]	log(τ_0) [s^{-1}]	$T_{g,100s}$ [K]
3	9.80	139.0	−13.5	177.1
5	8.00	153.7	−13.5	188.2
104	22.0	131.0	−13.5	211.8

[a]The value of $T_{g,100s}$ was calculated as an extrapolation to a relaxation time of 100 s.

In addition, both the relaxation time corresponding to the α'- and β-relaxation can be well described by an Arrhenius equation, $\tau = \tau_o \exp(E_a/kT)$, where E_a is the mean activation energy and k is the Boltzmann's constant. E_a and log(τ_o) were calculated and the resulting values are shown in Table 3. Values of E_a and log(τ_o) corresponding to α' relaxations are: 0.88 eV, −19.57 for 13PEO and 0.90 eV, −19.50 for 104PEO, respectively. So α'-relaxation is nearly identical for both samples.

Figure 5 shows the relaxation times corresponding to *n*PEO confined in GO. In addition, we included the relaxation times

Table 3. Activation Energy, E_a, and Preexponential Factor, log(τ_0), Corresponding to the β-Relaxation of Bulk PEO and the "Fast-Relaxation" of *n*PEO-GO As Obtained from the Arrhenius Equation Applied to the Data in Figures 4 and 5 (see Dotted Lines)

	β-relaxation bulk *n*PEO		fast-relaxation *n*PEO-GO	
n	E_a [eV]	log(τ_0) [s^{-1}]	E_a [eV]	log(τ_0) [s^{-1}]
3	0.44	−16.16	0.23	−10.30
5	0.37	−14.50	0.22	−9.90
13	0.41	−16.00	0.24	−10.60
104	0.29	−12.95	0.24	−10.50

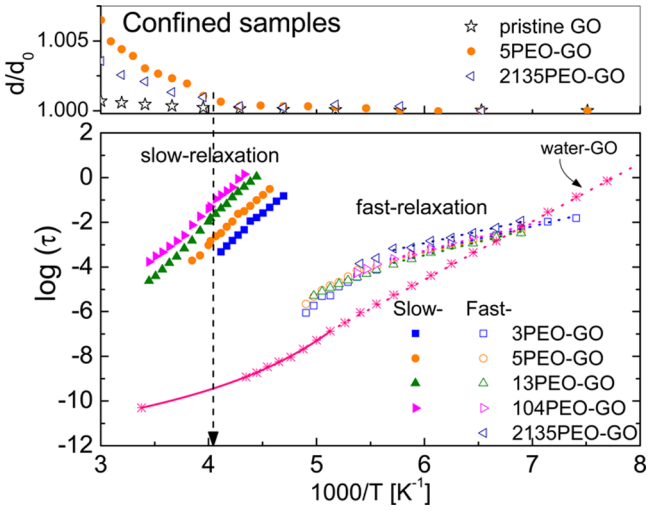

Figure 5. Upper panel: Relative interlayer distance of pristine GO and PEO-filled GO samples as a function of the inverse temperature (d and d_0 are the interlayer distance of expanded and nonexpanded layers, respectively. The following d_0 values were taken at 133 K: d_0 (GO) = 5.705 Å; d_0 (5PEO/GO) = 8.741 Å; d_0 (2135PEO/GO) = 8.901 Å). Bottom panel: Plot of the characteristic relaxation times of *n*PEO-GO. Fast-relaxation (open symbols) and slow-relaxation (full symbols) are shown. The dotted lines display fits to the Arrhenius equation for the fast-relaxation. Crosses represent the relaxation times of water confined in GO (water−GO sample, containing 25 wt % water) taken from ref 34. The arrow indicates the temperature at which an expansion of the interlayer distance occurs, which coincides with a change in the activation energy of the slow-relaxation.

obtained from isothermal measurements of a confined PEO with higher chain length, 2135PEO-GO (M_n = 100 000 g/mol). Note that isochronal dielectric data of this sample were previously reported in ref 39. Focusing on the "fast-relaxation", we can observe that relaxation times are very similar for all the samples, particularly the temperature dependence. At $T \sim 175$ K a stronger temperature variation of the relaxation times is observed. Below this temperature, relaxation times follow an Arrhenius behavior, whose corresponding values of activation energy and pre-exponential factor are shown in Table 3. An average activation energy of 0.23 eV is obtained for all the samples. In addition, the relaxation times show a crossover in temperature dependence at around 175 K. This crossover resembles one previously found by us in the study of the dynamics of water confined in GO.[34] However, when we compare the relaxation time data for 25 wt % water confined in GO with those found for *n*PEO (see Figure 5) it is clear that there is not a relationship. The water relaxation time is faster than that found in the current work for *n*PEO, the activation energy is markedly different and also the crossover temperature is higher than for confined *n*PEO.

Finally, we focus on the slow-relaxation shown in Figure 5. Relaxation times become higher by increasing the chain length. The temperature dependence is rather pronounced but it does not clearly follow a VFT behavior for an α-relaxation. Interestingly, we detected an abrupt change in the activation energy at 247 K, which seems to be directly correlated to the expansion of the GO interlayer distance as detected by XRD (see the upper panel of Figure 5). Note that this interlayer expansion occurs at the same temperature for short and long PEO chains (n = 5 and 2135, respectively) and that it is almost negligible in pristine GO.

dx.doi.org/10.1021/ma401373p | *Macromolecules* 2013, 46, 7932−7939

4. DISCUSSION

Polymer molecules confined in reduced spaces often exhibit properties that deviate from those of bulk materials. Although in other studies the comparison of the α- and β-relaxations of bulk and confined phases is straightforward, it is important to note that our previous studies on this system showed that the conformation of *n*PEO chains upon confinement differs from that of the bulk polymers (*n*PEO chains are forced to adopt a nearly planar conformation in a monolayer arrangement[40] and therefore the polymer chains no longer exhibit the helical structure observed for the bulk phase). In light of these findings, the relationship between the slow- and fast-relaxations detected in confinement with the α- and β-relaxations of bulk materials, respectively, is not directly evident. In the next subsections we will discuss the possible relationship between both relaxation processes.

4.1. Slow-Relaxation. As mentioned above, a calorimetric glass transition is not observed in the *n*PEO-GO specimens and consequently, the detection of an α-relaxation by BDS is not expected. In addition, previous studies on the dynamics of confined polymers have shown that the α-relaxation is generally faster than that of bulk if finite size effects are dominant.[9] According to our results, the slow-relaxation observed in *n*PEO-GO materials is much slower than the α-relaxation of their corresponding bulk *n*PEO. In addition, the characteristics of the slow-relaxation (shape and temperature dependence of the relaxation times) are markedly different from those expected for a conventional α-relaxation. Finally, this process appears very much overlapped with the conductivity contribution. For these reasons, the slow-relaxation could be associated with other phenomena different from an α-relaxation under confinement. For instance, it is well-known that heterogeneous systems can lead to interfacial polarization effects due to the difference in the dielectric properties of the components. These phenomena are supported by the observed change in the activation energy at the temperature at which an expansion of the GO interlayer occurs.

To gain further insight into the slow-relaxation process, dielectric modulus of confined samples were also analyzed. Figure 6 shows the dielectric loss modulus (M'') recorded isothermally at 240 K, a temperature at which the interlayer space of *n*PEO-GO samples remains stable. Note that M'' values can not be accurately compared due to uncertainties in the determination of the volume of powder-form samples inside the parallel plate capacitor. First of all, we observed that the slow-relaxation peak in M'' is better resolved than in the ε'' representation previously used. In the case of 3PEO-GO and 2135PEO-GO, the slow-relaxation peak is not well resolved due to an overlap with low frequency contributions and the presence of a background of relatively high intensity, respectively. Their approximate position is indicated with arrows in the figure. Notwithstanding the above, the effect of chain length on the peak position is clear in the rest of samples. Moreover, a concomitant increase of the low frequency contributions with increasing peak frequency is observed for the shortest PEO chains, which suggests that ionic conductivity plays an important role in the origin of the slow-relaxation as expected in the interfacial polarization phenomena. The effect of chain length on the slow-relaxation can be interpreted in terms of an important contribution of the hydroxyl end-groups of PEO chains to the ionic conductivity of the sample by favoring the ionic migration. The shorter the chains the higher the amount of hydroxyl end-groups in the sample, and therefore, the larger the ionic conductivity.

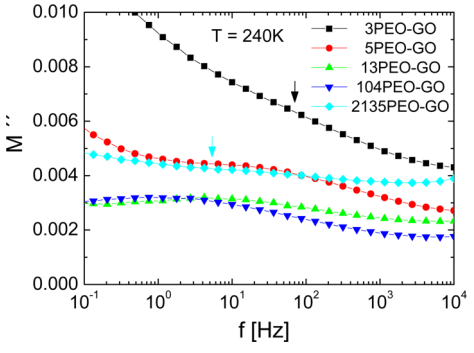

Figure 6. Dielectric loss modulus for *n*PEO-GO at 240 K. Arrows indicate an approximate position for the slow-relaxation peak in 3PEO-GO and 2135PEO-GO.

4.2. Fast-Relaxation. The relaxation times corresponding to the fast-relaxation present two main characteristics: $\tau(T)$ does not show much dependence on the chain length, and it shows an unexpected crossover at $T \sim 175$ K, where the temperature dependence becomes stronger at higher temperatures. Figure 7 shows the comparison between the relaxation times of the β-relaxation of bulk 13PEO and the fast-relaxation of 13PEO-GO. At a first glance, it could be possible to associate these two relaxations due to their close position in the relaxation map. However, the activation energy of the fast-relaxation in *n*PEO-GO is appreciably smaller than that of the β-relaxation in bulk *n*PEO (see Table 3). This result is very different from what is generally obtained for other confined systems investigated in the literature, where it has been found that the relaxation times associated with secondary relaxations are commonly not affected by confinement. Usually, β-relaxation undergoes a broadening due to confinement but the peak position in the ε'' spectra (and consequently the

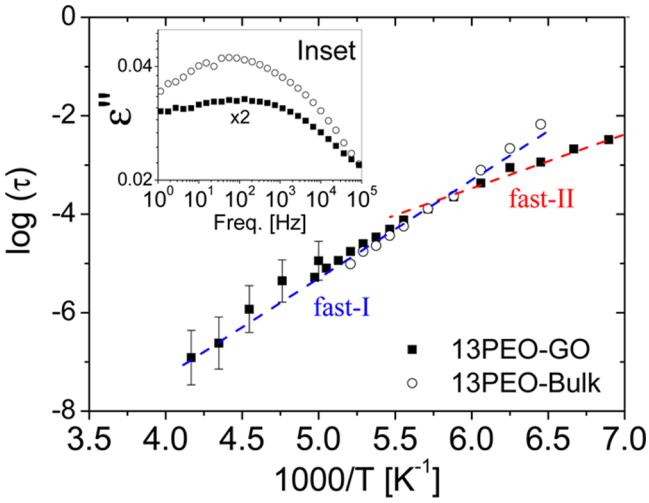

Figure 7. Temperature dependence of the relaxation times corresponding to the fast processes of bulk and confined 13PEO. Data from high frequency experiments are included with an estimated error bar. The dashed lines represent the Arrhenius fits of the fast-I and fast-II components for 13PEO-GO (see the text). Inset shows a direct comparison of the ε'' data of bulk and confined 13PEO at 160 K. To facilitate comparison, ε'' data of 13PEO-GO was multiplied by 2.

dx.doi.org/10.1021/ma401373p | Macromolecules 2013, 46, 7932−7939

activation energy) is not significantly affected.[21,22] A standard interpretation of this result is that a local motion can not be affected by confinement because of the small size of the moving unit. The situation in our system seems to be different and it is probably related to the changes in the chain conformation induced by the extreme 2D confinement in the GO interlayer space. In this sense, it is well established that conformational changes affect local barriers and therefore would also affect local molecular motions. The fact that the fast-relaxation for confined *n*PEO was found to be nearly independent of the chain length, strongly suggests that the molecular mechanism underlying this process would be characteristic of a particular molecular conformation. This situation can be promoted by the hydrogen bonds between *n*PEO ether groups and GO hydroxyl groups as well as between *n*PEO hydroxyl end-groups and GO epoxy groups, such that the local molecular environment becomes nearly unaffected by the chain length. The INS results already mentioned clearly support a common molecular conformation under confinement for all chain lengths.[40]

Despite previous arguments explaining the characteristics of the fast-relaxation for confined *n*PEO, it is not clear how to interpret the change in the behavior of the relaxation times at about 175 K, which is quite astonishing. As already mentioned, the crossover from a low temperature Arrhenius-like behavior toward stronger temperature dependence resembles the crossover from an Arrhenius to VFT observed/expected for the α-relaxation under confinement.[53,54] An alternative explanation for this crossover is that it stems from a simultaneous contribution of two local molecular mechanisms with quite different temperature dependence. In this framework, the detected ε'' peak, which is rather broad, would mainly reflect the fastest molecular motions at low temperatures, whereas the slowest one would be dominant at higher temperatures. Interestingly, the fast-relaxation peak at low temperatures looks quite asymmetric. It is significantly extended toward lower frequencies (see Figure 3), as expected from the previous interpretation. The possibility of the existence of two overlapping relaxation components for the fast-relaxation is also suggested by a significant intensity increase of the ε'' peak with the temperature. If the lower frequency component had a higher activation energy, the measured relaxation peak at higher temperatures would become narrower and more pronounced when the two peak frequencies approach to each other. Trying to confirm this scenario we have performed complementary dielectric experiments at higher frequencies (10^6–10^9 Hz) by using an Agilent rf impedance analyzer 4192B. However, due to the limited accuracy of the experiments in this high frequency range, only data for 13PEO-GO were actually reliable. Using these new data, we were able to evaluate the temperature dependence of the fast-relaxation ε'' peak in this sample up to 240 K. When these new data were included in the Arrhenius plot (see Figure 7), it became quite clear that a well-defined Arrhenius law can be established for the high temperature behavior. The activation energy in this range (0.41 eV) is nearly twice that at low temperatures and closer to that of the β-relaxation of the corresponding bulk (see Figure 7). Thus, the new picture that emerges is that the fast-relaxation for *n*PEO-GO stems from a combination of two distinct molecular motions named fast-I and fast-II components. The fast-I is similar in nature to that detected in the bulk and the fast-II is dominating the detected relaxation at the lowest temperatures once the previous one becomes very slow. The fast-II process is probably associated with the planar zigzag conformation of confined *n*PEO severely imposed by the geometrical confinement.

It is worthy mentioning that the fast-II component was not detected in our previous work,[39] where an isochronal representation was used for comparing the dynamics of confined 2135PEO with its bulk material. As can be seen in Figure S2 of the Supporting Information, the isochronal representation of 13PEO-GO data also do not exhibit the crossover already observed in the fast-relaxation at 175 K in the isothermal representation of Figure 7. Finally, it is also worth noting that the time scale of the fast-relaxation for confined *n*PEO is nearly independent of the chain length, in contrast to the behavior that we observed for the bulk polymer. These results strengthen our previous hypothesis based on high-resolution INS results suggesting the emergence of a new set of chain length scales primarily dictated by the presence of anchoring points on the GO substrate upon intercalation.[40]

Summarizing the dielectric results, the slow-relaxation was identified as originating from interfacial polarization phenomena, whereas the fast-relaxation was associated with local motions as those occurring in the β-relaxation of bulk PEO. At temperatures below 175 K, other molecular motions with much lower activation energy than that associated with the β-relaxation of bulk PEO become relevant, which can be solely associated with confined PEO chains. Unfortunately, a molecular picture of such motions is lacking. Finally, it is noteworthy to say that none of the dielectric relaxation processes detected in *n*PEO confined in the interlayer space of GO can be attributed to the segmental (α-) relaxation, which is ubiquitous in bulk polymers and other glass formers. This somehow surprising result is however in agreement with the absence of any detectable jump in the heat flow associated with the transformation between a liquid and a glass state. Taking this into account, the above-mentioned possibility of interpreting the absence of any detectable DSC glass transition in *n*PEO-GO as a result of the presence of extremely broad distributions of segmental relaxation times is uncertain. Thus, the question that arises is whether under extreme 2D confinement, as is the case of the investigated *n*PEO-GO systems, the cooperative character of the segmental motions can be lost. Such a situation would be certainly favored by the direct anchorage of the polymer chain segments to the GO layers through hydrogen bonding. The presence of this relatively strong polymer-GO interaction could be sufficient to prevent the general occurrence of cooperative motions involving a significant number of monomeric units.

CONCLUSIONS

By means of broadband dielectric spectroscopy we have shown that the dynamics of PEO is quite significantly modified upon the extreme 2D confinement in the interlayer space of GO compared to the bulk polymer. We observed two relaxations that we have called slow- and fast-relaxation. The slow-relaxation was assigned to interfacial polarization phenomena, whereas the fast-relaxation was attributed to two different local motions: fast-I and fast-II components with similar and lower activation energy than that of the β-relaxation of the bulk PEO, respectively. The motions of low activation energy dominate the detectable dielectric relaxations below ca. 175 K, and they might be associated with the predominance of planar zigzag conformations in *n*PEO/GO. We found that under confinement, the polymer chain length has a negligible effect on the local molecular motions in stark contrast to the behavior

observed for the β-relaxation of the bulk polymer. These findings are in agreement with our previous results obtained by high-resolution INS, where striking similarities in the INS spectra for all confined *n*PEO chains were observed such as the disappearance of collective vibrational modes and the emergence of specific bands related to the *trans*−*trans*−*trans* chain conformation.

■ ASSOCIATED CONTENT

Supporting Information

Supplementary BDS data for amorphous and semicrystalline 5PEO as well as the relaxation times for 13PEO-GO obtained from an isochronal representation. This material is available free of charge via the Internet at http://pubs.acs.org.

■ AUTHOR INFORMATION

Corresponding Author

*E-mail: (F.B.-B.) fbarroso@ehu.es.

Notes

The authors declare no competing financial interest.

■ ACKNOWLEDGMENTS

The authors gratefully acknowledge the support of the Spanish Ministry of Education, Project MAT2012-31088, and the Basque Government, Project IT-654-13.

■ REFERENCES

(1) Ediger, M. D.; Angell, C. A.; Nagel, S. R. *J. Phys. Chem.* **1996**, *100*, 13200−13212.
(2) Angell, C. A.; Ngai, K. L.; McKenna, G. B.; McMillan, P. F.; Martin, S. W. *J. Appl. Phys.* **2000**, *88*, 3113−3157.
(3) Debenedetti, P. G.; Stillinger, F. H. *Nature* **2001**, *410*, 259−267.
(4) Hempel, E.; Hempel, G.; Hensel, A.; Schick, C.; Donth, E. *J. Phys. Chem. B* **2000**, *104*, 2460−2466.
(5) Fischer, E. W.; Donth, E.; Steffen, W. *Phys. Rev. Lett.* **1992**, *68*, 2344−2346.
(6) Jackson, C. L.; McKenna, G. B. *J. Chem. Phys.* **1990**, *93*, 9002−9011.
(7) Jackson, C. L.; McKenna, G. B. *J. Non-Cryst. Solids* **1991**, *131*−*133*, 221−224.
(8) Alcoutlabi, M.; McKenna, G. B. *J. Phys.: Condens. Matter* **2005**, *17*, R461.
(9) Richert, R. *Annu. Rev. Phys. Chem.* **2011**, *62*, 65−84.
(10) Keddie, J. L.; Jones, R. A. L.; Cory, R. A. *Europhys. Lett.* **1994**, *27*, 59.
(11) Forrest, J. A.; Dalnoki-Veress, K.; Dutcher, J. R. *Phys. Rev. E* **1997**, *56*, 5705−5716.
(12) Serghei, A.; Tress, M.; Kremer, F. *Macromolecules* **2006**, *39*, 9385−9387.
(13) Fukao, K.; Miyamoto, Y. *Phys. Rev. E* **2000**, *61*, 1743−1754.
(14) Peter, S.; Napolitano, S.; Meyer, H.; Wübbenhorst, M.; Baschnagel, J. *Macromolecules* **2008**, *41*, 7729−7743.
(15) Napolitano, S.; Wubbenhorst, M. *Nat. Commun.* **2011**, *2*, 260.
(16) Serghei, A.; Huth, H.; Schick, C.; Kremer, F. *Macromolecules* **2008**, *41*, 3636−3639.
(17) Boucher, V. M.; Cangialosi, D.; Yin, H.; Schönhals, A.; Alegria, A.; Colmenero, J. *Soft Matter* **2012**, *8*, 5119−5122.
(18) Kremer, F.; Huwe, A.; Arndt, M.; Behrens, P.; Schwieger, W. *J. Phys.: Condens. Matter* **1999**, *11*, A175.
(19) Frunza, L.; Kosslick, H.; Frunza, S.; Schönhals, A. *J. Phys. Chem. B* **2002**, *106*, 9191−9194.
(20) Spange, S.; Gräser, A.; Huwe, A.; Kremer, F.; Tintemann, C.; Behrens, P. *Chem.—Eur. J.* **2001**, *7*, 3722−3728.
(21) Cerveny, S.; Mattsson, J.; Swenson, J.; Bergman, R. *J. Phys. Chem. B* **2004**, *108*, 11596−11603.
(22) Schwartz, G. A.; Bergman, R.; Swenson, J. *J. Chem. Phys.* **2004**, *120*, 5736−5744.
(23) Elmahdy, M. M.; Chrissopoulou, K.; Afratis, A.; Floudas, G.; Anastasiadis, S. H. *Macromolecules* **2006**, *39*, 5170−5173.
(24) Martín, J.; Krutyeva, M.; Monkenbusch, M.; Arbe, A.; Allgaier, J.; Radulescu, A.; Falus, P.; Maiz, J.; Mijangos, C.; Colmenero, J.; Richter, D. *Phys. Rev. Lett.* **2010**, *104*, 197801.
(25) Suzuki, Y.; Duran, H.; Steinhart, M.; Butt, H.-J.; Floudas, G. *Soft Matter* **2013**, *9*, 2621−2628.
(26) Zhang, C.; Guo, Y.; Priestley, R. D. *J. Polym. Sci., Part B: Polym. Phys.* **2013**, *51*, 574−586.
(27) Colmenero, J.; Arbe, A. *Soft Matter* **2007**, *3*, 1474−1485.
(28) Fragiadakis, D.; Runt, J. *Macromolecules* **2009**, *43*, 1028−1034.
(29) Willner, L.; Lund, R.; Monkenbusch, M.; Holderer, O.; Colmenero, J.; Richter, D. *Soft Matter* **2010**, *6*, 1559−1570.
(30) Wang, H. P.; Keum, J. K.; Hiltner, A.; Baer, E.; Freeman, B.; Rozanski, A.; Galeski, A. *Science* **2009**, *323*, 757−760.
(31) Barroso-Bujans, F.; Fernandez-Alonso, F.; Pomposo, J. A.; Cerveny, S.; Alegría, A.; Colmenero, J. *ACS Macro Lett.* **2012**, *1*, 550−554.
(32) Barroso-Bujans, F.; Fernandez-Alonso, F.; Pomposo, J. A.; Enciso, E.; Fierro, J. L. G.; Colmenero, J. *Carbon* **2012**, *50*, 5232−5241.
(33) Buchsteiner, A.; Lerf, A.; Pieper, J. *J. Phys. Chem. B* **2006**, *110*, 22328−22338.
(34) Cerveny, S.; Barroso-Bujans, F.; Alegría, A.; Colmenero, J. *J. Phys. Chem. C* **2010**, *114*, 2604−2612.
(35) Wang, D.-W.; Du, A.; Taran, E.; Lu, G. Q.; Gentle, I. R. *J. Mater. Chem.* **2012**, *22*, 21085−21091.
(36) Talyzin, A. V.; Luzan, S. M.; Szabó, T.; Chernyshev, D.; Dmitriev, V. *Carbon* **2011**, *49*, 1894−1899.
(37) Luzan, S. M.; Talyzin, A. V. *J. Phys. Chem. C* **2011**, *115*, 24611−24614.
(38) Barroso-Bujans, F.; Cerveny, S.; Alegría, A.; Colmenero, J. *Carbon* **2010**, *48*, 3277−3286.
(39) Barroso-Bujans, F.; Fernandez-Alonso, F.; Cerveny, S.; Parker, S. F.; Alegría, A.; Colmenero, J. *Soft Matter* **2011**, *7*, 7173−7176.
(40) Barroso-Bujans, F.; Fernandez-Alonso, F.; Cerveny, S.; Arrese-Igor, S.; Alegría, A.; Colmenero, J. *Macromolecules* **2012**, *45*, 3137−3144.
(41) Brodie, B. C. *Philos. Trans. R. Soc. London* **1859**, *149*, 249−259.
(42) Havriliak, S.; Negami, S. *J. Polym. Sci., Part C: Polym. Symp.* **1966**, *14*, 99−117.
(43) Cole, K. S.; Cole, R. H. *J. Chem. Phys.* **1942**, *10*, 98−105.
(44) Vaia, R. A.; Sauer, B. B.; Tse, O. K.; Giannelis, E. P. *J. Polym. Sci., Part B: Polym. Phys.* **1997**, *35*, 59−67.
(45) Miwa, Y.; Drews, A. R.; Schlick, S. *Macromolecules* **2008**, *41*, 4701−4708.
(46) Sanz, A.; Nogales, A.; Ezquerra, T. A.; Soccio, M.; Munari, A.; Lotti, N. *Macromolecules* **2009**, *43*, 671−679.
(47) Lund, R.; Alegria, A.; Goitandia, L.; Colmenero, J.; Gonzalez, M. A.; Lindner, P. *Macromolecules* **2008**, *41*, 1364−1376.
(48) Cerveny, S.; Zinck, P.; Terrier, M.; Arrese-Igor, S.; Alegría, A.; Colmenero, J. *Macromolecules* **2008**, *41*, 8669−8676.
(49) Viciosa, M. T.; Correia, N. T.; Sanchez, M. S. n.; Carvalho, A. L.; Romão, M. J.; Gómez Ribelles, J. L.; Dionísio, M. *J. Phys. Chem. B* **2009**, *113*, 14209−14217.
(50) Vogel, H. Das Temperaturabhängigkeitsgesetz der Viskosität von Flüssigkeiten. *Phys. Z.* **1921**, *22*, 645−646.
(51) Fulcher, G. S. *J. Am. Ceram. Soc.* **1925**, *8*, 339−355.
(52) Tammann, G.; Hesse, W. *Z. Anorg. Allg. Chem.* **1926**, *156*, 245−257.
(53) Floudas, G.; Paraskeva, S.; Hadjichristidis, N.; Fytas, G.; Chu, B.; Semenov, A. N. *J. Chem. Phys.* **1997**, *107*, 5502−5509.
(54) Turky, G.; Wolff, D.; Schönhals, A. *Macromol. Chem. Phys.* **2012**, *213*, 2420−2431.